Hindawi
Journal of Oncology
Volume 2021, Article ID 2042114, 13 pages
https://doi.org/10.1155/2021/2042114

Research Article

Identification of Prognostic Metabolism-Related Genes in Clear Cell Renal Cell Carcinoma

Yusa Chen, Yumei Liang, Ying Chen, Shaxi Ouyang, Kanghan Liu, and Wei Yin

Department of Nephrology, Hunan Provincial People's Hospital, The First Affiliated Hospital of Hunan Normal University, Changsha 410000, China

Correspondence should be addressed to Wei Yin; beau618618@163.com

Received 26 May 2021; Accepted 13 September 2021; Published 27 September 2021

Academic Editor: Zhixiong Liu

Background. Clear cell renal cell carcinoma (ccRCC) is a cancer with abnormal metabolism. The purpose of this study was to investigate the effect of metabolism-related genes on the prognosis of ccRCC patients. *Methods*. The data of ccRCC patients were downloaded from the TCGA and the GEO databases and clustered using the nonnegative matrix factorization method. The limma software package was used to analyze differences in gene expression. A random forest model was used to screen for important genes. A novel Riskscore model was established using multivariate regression. The model was evaluated based on the metabolic pathway, immune infiltration, immune checkpoint, and clinical characteristics. *Results*. According to metabolism-related genes, kidney clear cell carcinoma (KIRC) datasets downloaded from TCGA were clustered into two groups and showed significant differences in prognosis and immune infiltration. There were 667 differentially expressed genes between the two clusters, of which 408 were screened by univariate analysis. Finally, 12 differentially expressed genes (*MDK*, *SLC1A1*, *SGCB*, *C4orf3*, *MALAT1*, *PILRB*, *IGHG1*, *FZD1*, *IFITM1*, *MUC20*, *KRT80*, and *SALL1*) were filtered out using the random forest model. The model of Riskscore was obtained by multiplying the expression levels of these 12 genes with the corresponding coefficients of the multivariate regression. We found that the Riskscore correlated with the expression of these 12 genes; the high Riskscore matched the low survival rate verified in the verification set. The analysis found that the Riskscore model was associated with most of the metabolic processes, immune infiltration of cells such as plasma cells, immune checkpoints such as PD-1, and clinical characteristics such as M stage. *Conclusion*. We established a new Riskscore model for the prognosis of ccRCC based on metabolism. The genes in the model provided several novel targets for the study of ccRCC.

1. Introduction

Approximately four hundred thousand people are diagnosed with renal cell carcinoma (RCC) worldwide every year. Approximately 70% of these patients have clear cell RCC (ccRCC) [1], one of the most common malignancies of the urinary system [2]. Genetically, the continuous loss of multiple tumor suppressor genes leads to ccRCC [3]. Surgical resection is the main treatment for early-stage ccRCC, but approximately three out of ten patients have metastasis after resection [4]. ccRCC is not sensitive to radiotherapy and chemotherapy [5]; therefore, more effective targeted therapy is needed. Other studies have explored the possible molecular markers or therapeutic targets of ccRCC from different perspectives, such as autophagy associated long noncoding RNAs (lncRNAs) [6], methylation modification of m6A [7], DNA methylation [8], and immune invasion [9]. We set out to find new potential targets from a metabolic perspective.

Mutations in cancer cells can lead to metabolic reprogramming causing abnormal metabolic patterns to meet the different needs from normal cells for cancer proliferation and growth [10]. Increased aerobic glycolysis and impaired oxidative phosphorylation, known as the Warburg effect [11], occur in cancer. The research and development of many anticancer drugs are aimed at the changes in these metabolic pathways [12]. The transformation of renal epithelial cells into ccRCC leads to a decrease in the level of fatty acid oxidation and damage to the mitochondrial structure; the resulting accumulation of

glycogen and lipids is the cause of ccRCC transparency [13]. The upregulation of glycolysis pathway genes is a central event in the pathogenesis of ccRCC [14]. The research and development of many anticancer drugs are aimed at the changes in these metabolic pathways [12]. Further studies on the changes in metabolism in ccRCC are needed.

The random forest algorithm is a common machine-learning algorithm often used in cancer and biological research as a routine bioinformatics protocol; it was used to reduce the dimensions to screen more important genes. This method has been widely used in many different prognostic models of ccRCC such as chromatin-remodeling genes [15], DNA methylation patterns [16], and microRNA [17]. Cancer is usually accompanied by abnormal changes in metabolic patterns. Previous studies have also established prognostic models for healthy people and ccRCC patients from the perspective of metabolism [18]. Our study found some key gene differences between high-risk and low-risk ccRCC patients that were not previously noted by other researches, providing a new research target for a follow-up study.

It was recognized in as early as the 1960s that there is a relationship between immune infiltration and prognosis in different diseases [19]. The cells involved in immune infiltration are immune cells that appear in tumors and are divided into 22 types, such as T, B, NK, and plasma cells. For example, NK cells play a role in tumor immunity; receptor or coreceptor recognition of ligands on tumor cells can activate NK cells, resulting in targets with insufficient HLA I expression being killed [20]. The metabolism of NK cells is impaired in the tumor microenvironment [21]. In cancer, neutrophils may promote tumor progression, in part by producing reactive oxygen species (ROS) [22]. The rewiring of other metabolic pathways in neutrophils may affect their tumorigenesis/metastasis promoting function [23]; such pathways are the main components of nontumor constituents in the tumor microenvironment, and different types of malignant tumors often show different features of immune cell subsets [24]. The prognostic significance of T cell tumor infiltration has been widely accepted [25]. Immune checkpoints refer to the set of inhibitory pathways possessed by immune cells to regulate and control the durability of the immune response while maintaining self-tolerance [26]. Many successful immunotherapies targeting these checkpoints are already available to treat ccRCC [27].

In this study, by clustering the cancer genome atlas (TCGA) kidney clear cell carcinoma (KIRC) datasets according to metabolic patterns and screening differentially expressed genes of two clusters, we constructed and verified a Riskscore model and analyzed the relationships between Riskscore and metabolic pathway, immune infiltration, immune checkpoint, and clinical features.

2. Methods

2.1. Datasets and Preprocessing. The workflow of this study is presented in Supplementary Figure S1. The phenotype datasets and RNA sequencing datasets of TCGA Kidney Clear Cell Carcinoma (KIRC) were downloaded from UCSC Xena (https://xenabrowser.net/). Then, the number of fragments per kilobase million fragments (FPKM) was converted to transcript/value per million-word node (TPM). The microarray dataset GSE29609 ($n = 30$) was used as an external validation set accessed from the Gene Expression Omnibus (GEO; https://www.ncbi.nlm.nih.gov/geo/). Affymetrix was used to generate raw data of the microarray dataset and quantile normalization and background correction of these data were performed using the rapid motor adaptation algorithm in the affy package. The clinicopathologic features (gender, age, grade, stage, and status) of the TCGA KIRC dataset were sorted and are shown in Supplementary Table S1.

2.2. KIRC Metabolic Gene Clustered. The 2752 metabolism-related genes were obtained from a previous study [28]. A total of 2585 genes were identified in TCGA data. Then, 1416 genes were screened by a univariate cox, and KIRC data were classified by the nonnegative matrix factorization clustering method to determine the metabolism-related patterns; datasets of patients were clustered for further analysis.

2.3. Immune Infiltration and Pathway Analysis. The type and number of immune cells in KIRC samples were quantified using the cell-type identification by estimating relative subsets of known RNA transcripts algorithm [29] to compare the differences in immune infiltration in different cluster categories or risk groups. Gene set variation analysis was used to calculate the activity of the metabolic pathway using 114 metabolic pathway sets [29].

2.4. Establishment of the Metabolic Riskscore Model. The limma package was used to identify the genes related to metabolism ($P < 0.05$ and $|\text{logfc}| > 1.5$); univariate screening was performed, and random survival forest was used for further screening [30]. The Riskscore was the sum of the gene expression value * regression coefficient (Riskscore = (0.1186* *MDK*) + (−0.0505* *SLC1A1*) + (−0.094* *SGCB*) + (−0.1992* *C4orf3*) + (0.1986* *MALAT1*) + (0.1051* *PILRB*) + (0.0142* *IGHG1*) + (−0.0541* *FZD1*) + (0.2203* *IFIT M1*) + (−0.1682* *MUC20*) + (0.1104* *KRT80*) + (−0.2114* *SALL1*)). The patients were divided into high-risk and low-risk groups using the surv_cutpoint method of the survminer package.

2.5. Cell Culture. A human ccRCC cell line (ZQ0339), CAKI-1, was cultured in McCoy's 5A medium (ZQ-1000). The cell line and the medium above were purchased from Shanghai Zhong Qiao Xin Zhou Biotechnology Co., Ltd. A normal human kidney proximal tubular cell line (CL-0109), HK-2, and its special medium (CM-0109) were purchased from Procell Life Science & Technology Co., Ltd. These cells were cultured at 5% CO_2 and 37°C. The medium contained 10% FBS (Gibco) and 1% Penicillin-Streptomycin Solution (C0222, Beyotime).

2.6. Quantitative Real-Time PCR (qRT-PCR). Relative RNA expressions of *SLC1A1*, *MALAT1, FZD1,* and *SALL1* in HK-2 and CAKI-1 cell lines were detected by qRT-PCR. The total RNA of cells was isolated by TRIzol® (15596026, Thermo) and reverse-transcribed to cDNA by HiFiScript cDNA Synthesis Kit (CW2569, Cwbio). qPCR amplification was performed using UltraSYBR Mixture (CW2601, Cwbio) with QuantStudio™ 1 Real-Time PCR System (Thermo), and the cycling conditions were followed by the operating instructions. The sequences of the primers used in this study are shown in Table 1. The expression of β-actin was selected as an internal reference, and the relative RNA expression of genes was calculated by the $2^{-\Delta\Delta}$ CT method (the expression fold of genes in HK-2 was regarded as 1, respectively)

2.7. Statistical Analyses. Before the unpaired Student's *t*-test was used to compare the differences between the two groups, the Shapiro–Wilk test was used to detect whether the variables were normally distributed. If they did not conform to the normal distribution, the Wilcoxon test was used to compare the differences between the groups. Correlation coefficients were calculated using the Pearson correlation analysis and distance correlation analysis. The datasets of patients were divided into high-risk and low-risk groups based on dichotomy. The data were visualized using ggplot2 (a package for R). Survival curves of subgroups were generated by the Kaplan–Meier method. The statistical significance of differences in each dataset was identified using the log-rank test. Survival curves were generated by survminer (a package for R); heat maps were generated using pheatmap. All statistical analyses above were performed in the environment of R 3.6.1. All statistical tests were two-sided and considered statistically significant when the *P* value was <0.05. Column charts of relative RNA expressions were drawn by GraphPad Prism 8.0.2.

3. Results

3.1. Two Groups of Patients Clustered by Metabolic Patterns Had a Different Prognosis. According to the metabolic genes, ccRCC patients were clustered into two groups (Figure 1(a)). It is suitable to divide the samples into 2 clusters rather than more clusters (Supplementary Figure S2). There were significant differences in the results of survival analysis between the two groups (Figure 1(b)). The distribution of immune cells in the two groups is shown in Figure 1(c). The results showed a significant difference between the two groups in NK cells activated, T cells follicular helper, B cells memory, neutrophils, dendritic cells activated, T cells CD4 memory activated, eosinophils, macrophages M1, B cells naive, and plasma cells. There was a significant difference in certainty between the two groups.

3.2. The Riskscore Model Was Established according to the Differentially Expressed Genes: the Higher the Score, the Worse the Prognosis. To study the prognosis of ccRCC based on metabolism, we established a Riskscore model according to the following steps. First, by analyzing the differential expression of metabolism-related genes between the above two categories, 667 candidate genes (Supplementary Table S2) were initially obtained; 408 genes (Supplementary Table S3) were left after univariate screening. Finally, 12 genes were obtained using the random forest algorithm (Figure 2(a)): *MDK*, *SLC1A1*, *SGCB*, *C4orf3*, *MALAT1*, *PILRB*, *IGHG1*, *FZD1*, *IFITM1*, *MUC20*, *KRT80*, and *SALL1*. The Riskscore model for these 12 genes was established using the multivariate Cox method. The Riskscore of each sample was calculated by the sum of multiplying the gene expression in the sample with their coefficient (the weight calculated by the Cox regression model). Then, we analyzed the correlation between Riskscores and the above 12 genes and ranked the samples according to the model score to create a heat map. Figure 2(b) shows that these 12 genes have statistically significant Riskscores. The expression trends of six upregulated genes, *MDK*, *MALAT1*, *PILRB*, *IGHG1*, *IFITM1*, *KRT80*, and six downregulated genes, *SLC1A1*, *SGCB*, *C4orf3*, *FZD1*, *MUC20*, and *SALL1*, were consistent with the positive and negative coefficients in the model. We chose 4 genes, *SLC1A1*, *MALAT1*, *FZD1*, and *SALL1*, performed survival analysis, and compared the different expressions between HK-2 cells and CAKI-1 cells, to verify their importance. Patients with low *SLC1A1*, *FZD1*, or *SALL1* expression or high *MALAT1* expression have a poor prognosis (Figure 2(c) and Figure S3). Compared with HK-2 cells, *SLC1A1*, *FZD1*, and *SALL1* were low-expressed, while *MALAT1* was high-expressed in CAKI-1 cells (Figure 2(d)). The survival analysis of the Riskscore model in the TCGA dataset (Figure 2(e)) and independent validation set (Figure 2(f)) showed that the higher the Riskscore, the worse the prognosis of patients; the *P* values of <0.05 document statistical significance. This Riskscore model could be used to predict the prognosis of ccRCC.

3.3. Riskscore and Different Metabolic Patterns between ccRCC Samples. The results of the correlation analysis between Riskscore and the activities of 114 metabolic pathways are shown in Figure 3. The Riskscore was negatively correlated with carbohydrate metabolism pathways such as glycolysis, gluconeogenesis, pyruvate metabolism, citric acid cycle, oxidative phosphorylation, pentose and glucuronate interconversions, and pentose phosphate and was negatively correlated with amino acid metabolism pathways such as glycine, serine and threonine metabolism, alanine, aspartate and glutamate metabolism, homocysteine biosynthesis, methionine cycle, cysteine and methionine metabolism, and kynurenine metabolism. The Riskscore was also negatively correlated with lipid metabolism pathways such as fatty acid degradation, glycerolipid metabolism, glycerophospholipid metabolism, steroid hormone metabolism, and steroid hormone biosynthesis, and negatively correlated with purine metabolism, pyrimidine metabolism, and purine biosynthesis. Riskscore was also negatively correlated with remethylation, vitamin K, retinol metabolism, and other

Table 1: Primers used in this study.

Primers	Sequences	Product length
SLC1A1-F	5′- TGAAGCCTCCCAGCGATCCAG -3′	142 bp
SLC1A1-R	5′- ATCAAGCCCAGGACGTTTATGCC -3′	
MALAT1-F	5′- ACTGTTCTGATCCCGCTGCT -3′	136 bp
MALAT1-R	5′- CCTCAACACTCAGCCTTTATCACT -3′	
FZD1-F	5′- ACCAACAGCAAACAAGGGGA -3′	163 bp
FZD1-R	5′- GGAGCCTGCGAAAGAGAGTT -3′	
SALL1-F	5′- AAACGGACGGGGAAAGTGTC -3′	180 bp
SALL1-R	5′- CAAAGAACTCGGCACAGCAC -3′	
β-Actin-F	5′- ACCCTGAAGTACCCCATCGAG -3′	224 bp
β-Actin-R	5′- AGCACAGCCTGGATAGCAAC -3′	

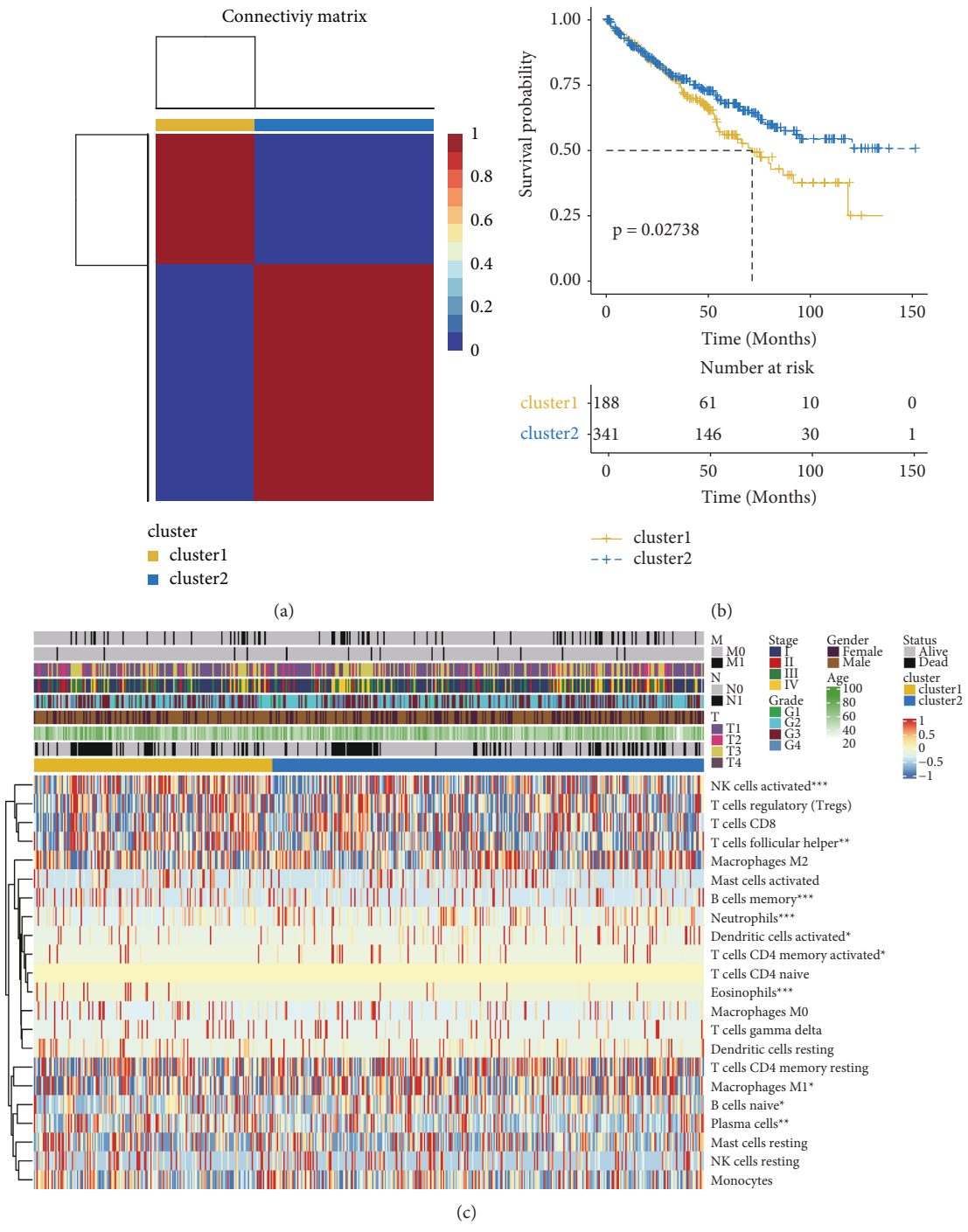

Figure 1: Clustering by metabolic genes. (a) Samples grouped into two categories. (b) Survival analysis of these two categories. (c) Distribution of samples and immune cells.

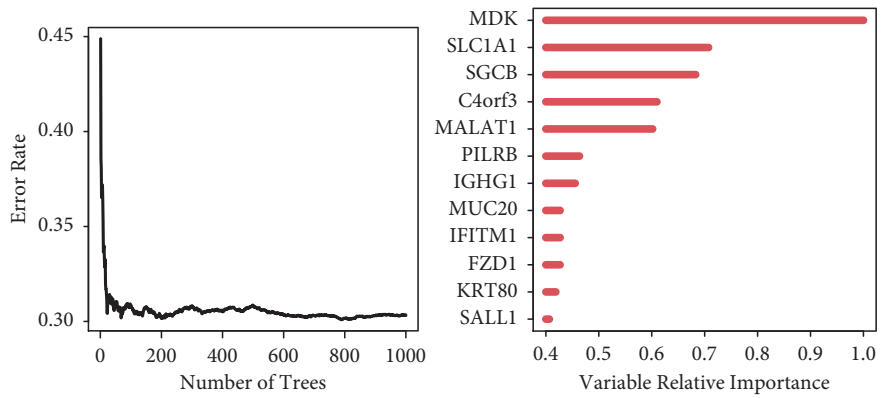

(a)

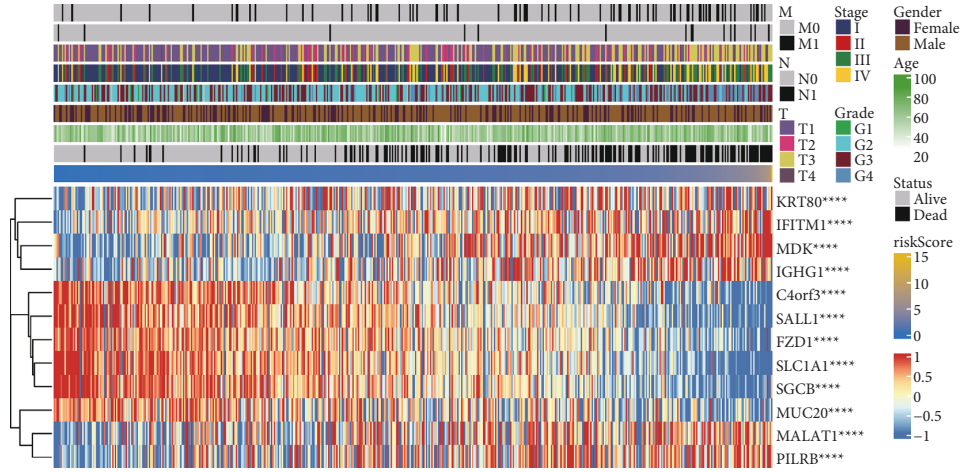

(b)

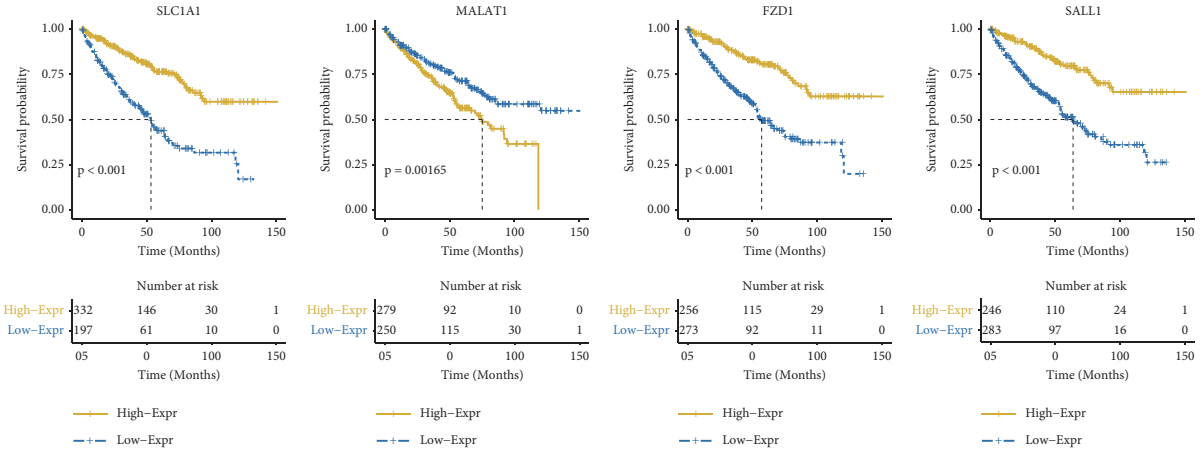

(c)

Figure 2: Continued.

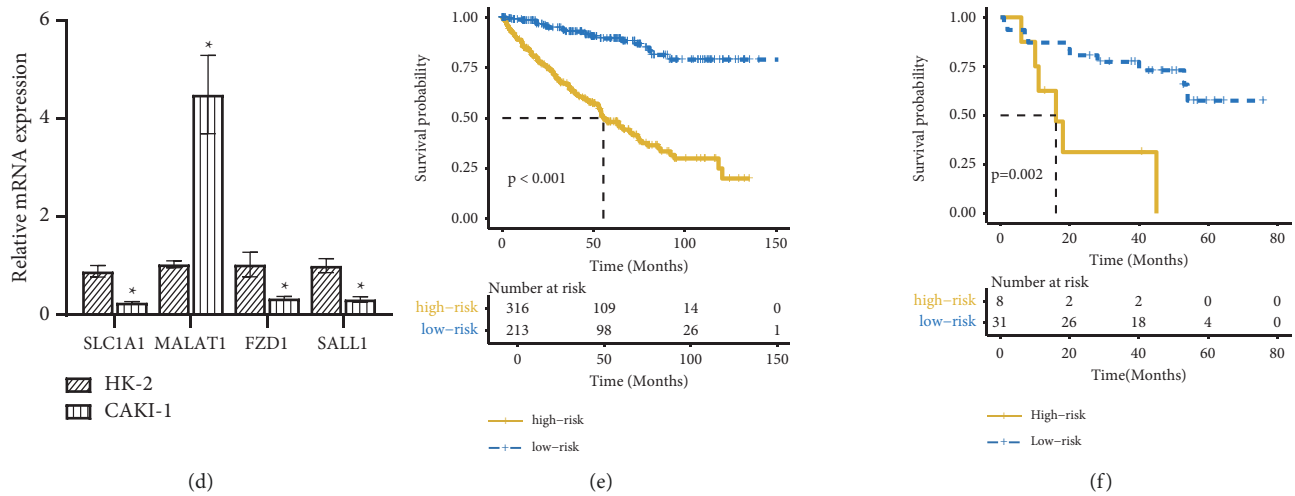

Figure 2: Establishment and verification of the prognosis score (Riskscore). (a) Error rate for the random trees and importance values for the 12 metabolism-related genes. (b) Riskscore modeling score, clinical characteristics, and specific expression of 12 genes. (c) Survival analysis of *FZD1*, *SALL1*, *SLC1A1*, and *MALAT1*. (d) Relative mRNA expressions of *FZD1*, *SALL1*, *SLC1A1*, and *MALAT1* in HK-2 (normal cells) and CAKI-1 (cell models of ccRCC). (e) Survival analysis of Riskscore in the TCGA datasets (KIRC). (f) Survival analysis of Riskscore in the independent verification set (GSE29609). *Compared with the HK-2 group, $P < 0.05$.

pathways. But there were few pathways positively correlated with Riskscore, such as transsulfuration, thromboxane biosynthesis, linoleic acid metabolism, alpha-linoleic acid metabolism, cyclooxygenase arachidonic acid metabolism, and retinoic acid metabolism, etc. It can be seen that our Riskscore is related to most metabolic processes and is mainly negatively correlated, involving almost every category of metabolism.

3.4. Relationship between Immune Infiltration and Immune Regulatory Factors in ccRCC Riskscore. To explore the relationship between Riskscore and immune infiltration, we divided the samples into two groups: high-Riskscore and low-Riskscore (Figure 4(a)). There were significant Riskscore differences in immune cells, including macrophages M0, macrophages M2, mast cells activated, mast cells resting, monocytes, NK cells resting, plasma cells, T cells CD4 memory activated, T cells CD4 memory resting, T cells CD8, T cells follicular helper, and T cells regulatory (Tregs). To explore the relationship between Riskscore and immune regulatory factors, we analyzed the correlation between Riskscore and immune inhibitors and immune stimulators and created a heat map (Figure 4(b)). The results show that our Riskscore model was related to immune inhibitors such as *ADORA2A*, *BTLA*, *CD96*, *CTLA4*, *HAVCR2*, *IDO1*, *IL10RB*, *KDR*, *KIR2DL1*, *KIR2DL3*, *LAG3*, *PDCD1*, *TGFB1*, *TGFBR1*, and *TIGIT*, and related to immune stimulators such as *CD27*, *CD80*, *ENTPD1*, *HHLA2*, *ICOS*, *ICOSLG*, *IL2RA*, *IL6*, *IL6R*, *KLRC1*, *KLRK1*, *LTA*, *MICB*, *NT5E*, *RAET1E*, *TMIGD2*, *TNFRSF13B*, *TNFRSF13C*, *TNFRSF14*, *TNFRSF17*, *TNFRSF18*, *TNFRSF25*, *TNFRSF8*, *TNFRSF9*, *TNFSF13*, *TNFSF13B*, *TNFSF14*, *TNFSF15*, *TNFSF18*, *TNFSF4*, and *ULBP1*. The Riskscore model we constructed was related to the immune infiltration and immune checkpoints.

3.5. Relationship between Riskscore and Clinical Features of ccRCC. To analyze the relationship between different clinical characteristics and Riskscore model, we first classified the data according to clinical characteristics. The results of the data analysis showed no significant difference in Riskscore among patients of different ages or genders, but there was a significant difference in Riskscore among samples with different M stage, N stage, T stage, grade, stage, and status (Figure 5). Univariate and multivariate analyses of clinical features and Riskscores are shown in Table 2. Univariate analysis showed that the Riskscore was significantly correlated with all clinical features except gender, while multivariate analysis showed that the Riskscore was significantly correlated with age and M stage. The results above indicated that Riskscores based on these 12 metabolism-related genes were a feasible prognostic factor in different populations.

4. Discussion

Metabolic reprogramming usually occurs in tumors. Compared with other cancers, studies tend to regard ccRCC as a metabolic disease [31, 32]. Metabonomics experiments have confirmed that there are significant changes in metabolic patterns in ccRCC, such as the rapid destruction of metabolic pathways of energy, amino acids, creatinine, and uric acid [33]. Many studies have evaluated the prognosis and diagnosis of ccRCC from the perspective of metabolic patterns [2] and treatment of ccRCC by reversing the abnormal metabolic pattern [34]. Our study has established a metabolic model to assess the prognosis of ccRCC and identified several genes related to the disease that were not considered previously.

Among the genes we selected to construct the Riskscore model, *SLC1A1* [35], *FZD1* [36], and *SALL1* [37] were downregulated in ccRCC, while *MALAT1* [38] was

Figure 3: Relationship between Riskscore and metabolic patterns. The correlation analyses between Riskscore and the activity of 114 metabolic pathways.

upregulated; there are specific clinical trials to verify their relationship with ccRCC. For example, *MALAT1* is a lncRNA that acts as a marker in various cancers [39], and miR-182-5p can reduce the proliferation of ccRCC by binding with *MALAT1* [38]. *C4orf3* [40] and *MDK* [41] were also used as markers to evaluate ccRCC. Research on the remaining genes in ccRCC is rare, although these genes play important roles in other cancers.

It seems that cancers prefer glycolysis that does not require oxygen consumption and does not involve pyruvate metabolism [42], and this phenomenon was confirmed by isotope experiments in ccRCC [43]. Oxidative phosphorylation is not high in ccRCC [4], and the TCA cycle in ccRCC is also reduced, differing from the metabolic pattern of the human brain and lung tumors [43]. The inhibition of gluconeogenesis and increased glycolysis are common in ccRCC [44]. In more than 600 cases of ccRCC, the level of fructose 1,6-bisphosphatase 1 (FBP1), a gluconeogenic enzyme, was reduced and was related to the poor prognosis of this disease [45]. In addition to the glycolysis pathway, the negative trends of our Riskscore model were consistent with those reported above for carbohydrate metabolism. Serine and threonine that often appear at protein kinase phosphorylation sites have hydroxyl groups in their structures. Although serine and glycine are nonessential amino acids, many cells still rely on exogenous serine to achieve optimal growth. Some studies have attempted to reduce the intake of amino acids in the diet to alleviate cancer [46]. The tryptophan level in ccRCC was decreased and its metabolism was strikingly linked to the kynurenine pathway [32].

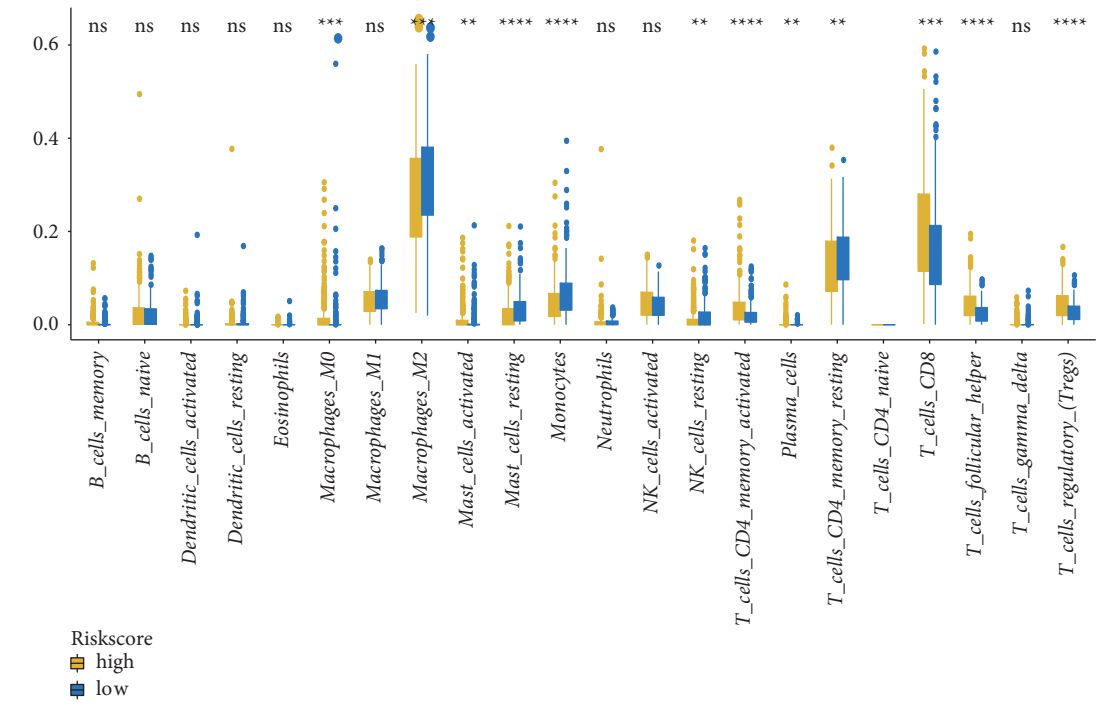

(a)

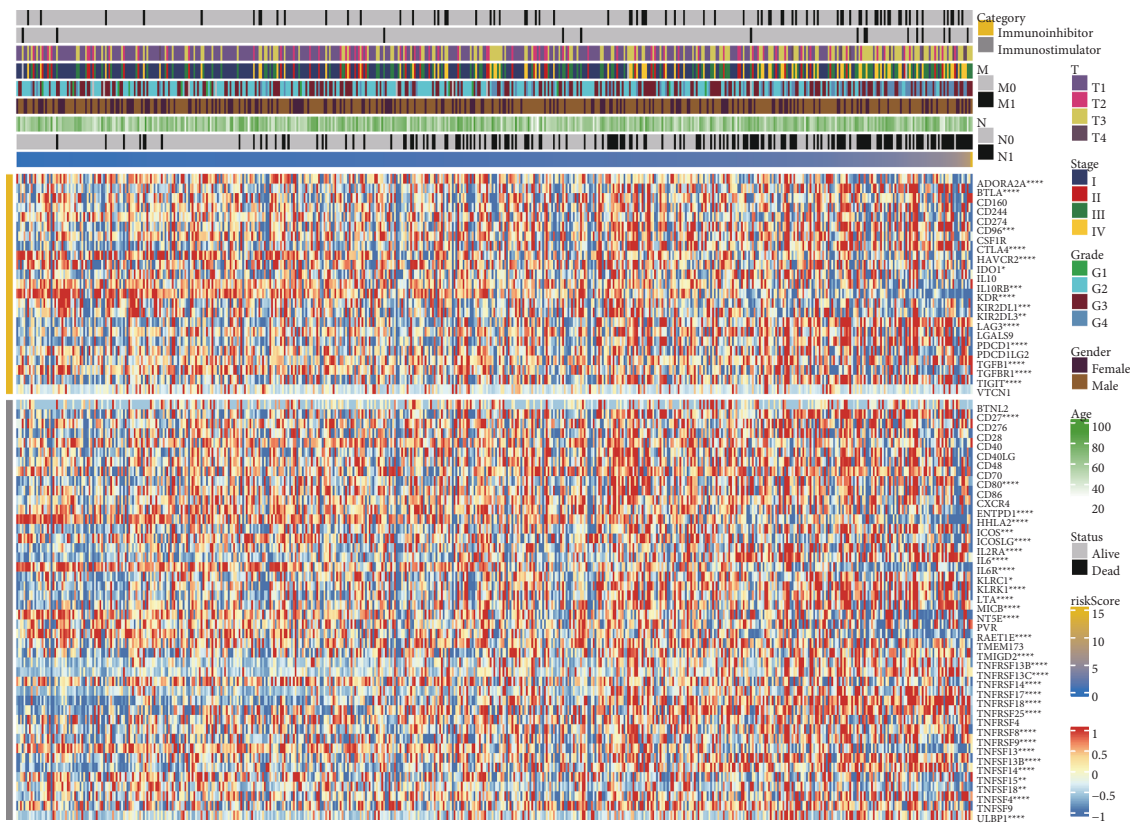

(b)

Figure 4: Relationship between Riskscore, immune infiltration, and immune checkpoints. (a) The high- and low-Riskscores of immune infiltrations. (b) Correlation between Riskscore and expression of immune regulatory factors.

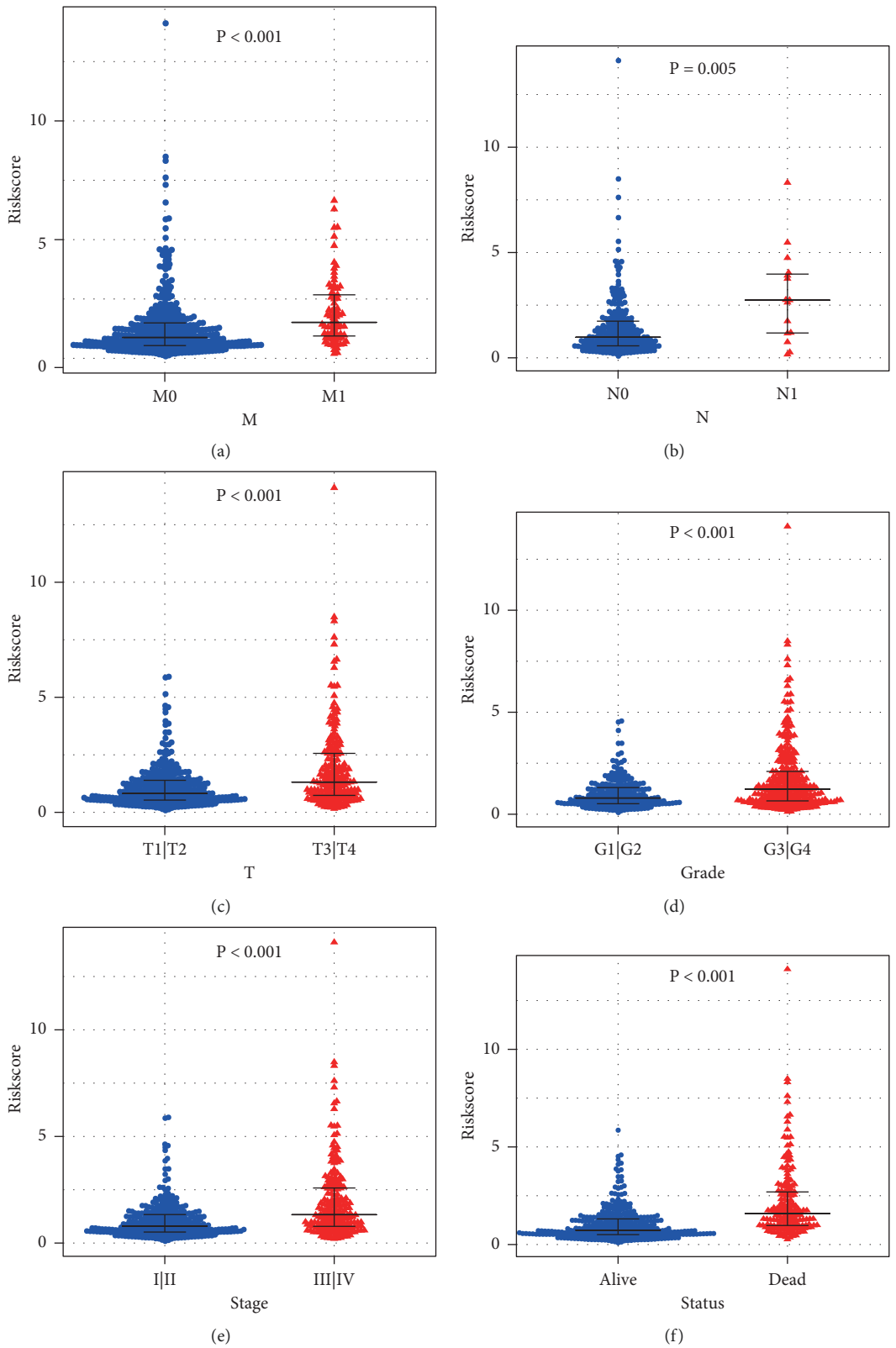

Figure 5: Continued.

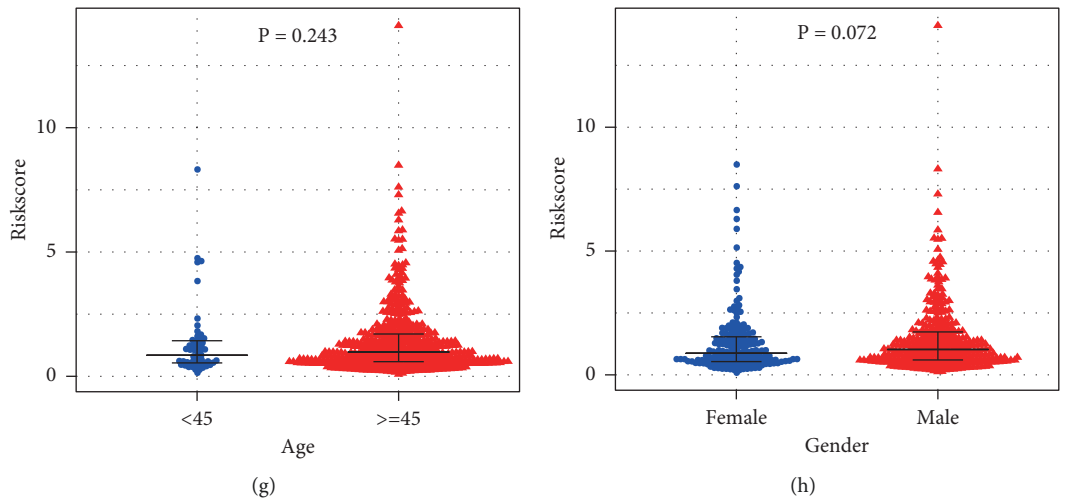

Figure 5: Difference in Riskscore model analyses for different clinical characteristics. (a) Different distributions of Riskscore in M0 and M1 stages. (b) Riskscore distribution among N0 and N1 stages. (c) Different distributions of Riskscore in T1 + T2 stage and T3 + T4 stages. (d) Riskscore distribution in G1 + G2 grade and G3 + G4 grade. (e) Riskscore distribution in stage I + stage II and stage III + stage IV. (f) Different distributions of Riskscore in alive and dead. (g) Different Riskscore distributions by age. (h) Different Riskscore by gender.

Table 2: Univariate and multivariate analyses of Riskscore and clinicopathological features with overall survival in TCGA KIRC cohort.

Characteristics	Univariate analysis HR (95% CI)	*P* value	Multivariate analysis HR (95% CI)	*P* value
Riskscore	1.317 (1.249–1.389)	<0.001	1.216 (1.118–1.323)	<0.001
Age	1.030 (1.017–1.043)	<0.001	1.031 (1.012–1.052)	0.002
Gender	0.949 (0.696–1.294)	0.742	1.314 (0.839–2.059)	0.233
Grade	2.578 (1.835–3.624)	<0.001	1.401 (0.843–2.328)	0.193
Stage	3.804 (2.772–5.221)	<0.001	1.266 (0.491–3.266)	0.625
T stage	3.119 (2.303–4.225)	<0.001	1.184 (0.515–2.722)	0.691
N stage	3.394 (1.754–6.567)	<0.001	1.582 (0.762–3.285)	0.218
M stage	4.283 (3.131–5.860)	<0.001	3.109 (1.823–5.303)	<0.001

Kynurenine metastasis of tumor cells can upregulate programmed cell death-1 (PD-1) in T cells [47]. The significant increase in glutathione (GSH), a reactive oxygen species (ROS) scavenger, has been identified as a marker of RCC. Demand for cysteine also increases in ccRCC. Cysteine is synthesized via transsulfuration. The flux of the pentose phosphate pathway in ccRCC increases [45]. In addition to the pentose phosphate pathway and kynurenine pathway, the negative trends of our Riskscore model were consistent with the above reports on amino acid metabolism, and the positive trends of our Riskscore model and transsulfuration were also consistent with these reports. Lipid accumulation in ccRCC causes hypertrophy caused by impaired lipid metabolism [42, 48], mainly due to inhibition of β-oxidation [13, 48] and impairment of fatty acid degradation [48]. The negative trends of our Riskscore model were consistent with these reports on lipid metabolism. The expression of NT5E and ENTPD1, factors related to purine and pyrimidine metabolism, increases in ccRCC [49]. The negative trends of our Riskscore model were opposite to the above-reported nucleotide metabolism.

The effects of NK cells and neutrophils were related to the two studies clusters, but there were no significant differences between high and low Riskscores. M1 macrophages can inhibit tumors, whereas polarized M2 macrophages can promote tumors [50]. Tumor cells and macrophages produce complement C1q to promote tumor growth [51]. Consistent with the Riskscores trends, M0 macrophages and T follicle helper cells in high-risk patients were higher than those in low-risk patients [52]. However, in our study, cells with a low-Riskscore had more M2 macrophages in ccRCC. $CD138^+$ plasma cells may secrete antibodies or act as Breg cells and promote tumor growth [53]. Consistent with this trend, our study found that the higher the Riskscore, the higher the number of plasma cells present. Activated $CD4^+$ memory T lymphocytes can target antigenic tumor cells, inhibit tumor growth, and play an active regulatory role in anti-tumor immunity [54]. However, in our study, the higher the Riskscore, the more of these two cell types were involved. There may be cooperation between immune cells that increases the complexity, and even the immune cells may be further divided into more subtypes, so the observation may not be simply related to the number of cells of a given type. The overall survival and progression-free survival of patients with ccRCC and Hodgkin's lymphoma with severe $CD8^+$ T cell infiltration were significantly

shorter. However, in some ccRCC patients with a "normal" immune environment, oligoclonal CD8 T cells express perforin. A high density of $CD8^+$ T cells is associated with a good prognosis in this subgroup [55]. The trends of our Riskscore model were consistent with those reported above.

The growth and progression of cancer are associated with immunosuppression [56]. Studies have found that immune inhibitors such as *LAG3* [27, 52], *BTLA* [27], *PD-1* (*PDCD1*) [52], and *CTLA-4* [52], or immunostimulators like *TNFSF13B* [57] play important roles in ccRCC. Our Riskscore was related to the immune checkpoints, which provides a new way to explore the mechanism of ccRCC.

The pattern of metabolism in ccRCC cells influences immune cells. For example, sulfatide, a product of ether lipid metabolism, accumulates in ccRCC, which could combine with platelets and evade cytotoxicity mediated by natural killer cells and immune surveillance [58]. In our study, we found that the effect of CD8 T cells was significantly higher in the high-Riskscore group (Figure 4(a)). Effector T cells require a high rate of glucose metabolism, while cancer cells inhibit T cells through using up nutrition and producing harmful components such as lactic acid. Although many $CD8^+$ T cells are involved in ccRCC, they cannot take glucose or glycolysis effectively [59]. Glutamine addiction is a characteristic of ccRCC; running out of glutamine in the tumor microenvironment leads to the secretion of IL-23 by macrophages, activating Treg responses, and thereby suppressing the anti-tumor toxicity of T cells [60].

Different types of cells are distributed in different parts of many tumors, including ccRCC. The heterogeneity of cell type may directly lead to the heterogeneity of metabolism in different parts of the same tumor; for example, the clear cells in ccRCC should respond to angiogenesis and glycolysis inhibitors, while eosinophilic components in ccRCC may benefit from mTOR or glutaminase inhibition [61]. Although the Riskscore model was based on the expression differences of metabolic genes, and the relationship between the Riskscore model and the prognosis was roughly in line with our prediction after verification, the relationship between our model and metabolic pathways was not the same as the actual changes in ccRCC metabolic patterns, indicating the metabolic complexity of different stages of ccRCC. Our study suggests that these genes might be important, but further studies are needed to clarify and validate the detailed mechanism behind their indicated significance.

5. Conclusion

In this study, we constructed a Riskscore model with 12 metabolism-related genes. The higher the score, the worse the prognosis. The Riskscore is closely related to metabolism, immune infiltration, and immune checkpoints, which can be used as one of the potential prognostic criteria of ccRCC.

Data Availability

All the data used in this study have been listed in the main text of the article. TCGA KIRC datasets were downloaded from UCSC Xena (https://xenabrowser.net/) as the training dataset for ccRCC, while GSE29609 was downloaded from the GEO database (https://www.ncbi.nlm.nih.gov/geo/) as the independent validation dataset.

Conflicts of Interest

The authors declare that there are no conflicts of interest regarding the publication of this paper.

Acknowledgments

This research was supported by the Hunan Provincial Health Committee Science Research Project (No. 20200387), Hunan Provincial People's Hospital Doctoral Sustentation Fund (No. BSJJ202006), and Hunan Clinical Research Center for Chronic Kidney Disease (No. 2019SK4009).

Supplementary Materials

Supplementary Table S1: clinicopathologic parameters of TCGA KIRC dataset. Supplementary Table S2: DEG to clusters. Supplementary Table S3: univar result after limma final. Supplementary Figure S1: flowchart of data collection and analysis in this study. Supplementary Figure S2: the relationship between the cophenetic coefficient and the number of clusters. Supplementary Figure S3: survival analysis of *MDK*, *SGCB*, *C4orf3*, *PILRB*, *IGHG1*, *IFITM1*, *MUC20*, and *KRT80*. (*Supplementary Materials*)

References

[1] E. Jonasch, C. L. Walker, and W. K. Rathmell, "Clear cell renal cell carcinoma ontogeny and mechanisms of lethality," *Nature Reviews Nephrology*, vol. 17, no. 4, pp. 245–261, 2021.

[2] T. Xu, H. Ruan, Z. Song et al., "Identification of CXCL13 as a potential biomarker in clear cell renal cell carcinoma via comprehensive bioinformatics analysis," *Biomedicine & Pharmacotherapy*, vol. 118, Article ID 109264, 2019.

[3] J. J. Hsieh, V. H. Le, T. Oyama, C. J. Ricketts, T. H. Ho, and E. H. Cheng, "Chromosome 3p loss-orchestrated VHL, HIF, and epigenetic deregulation in clear cell renal cell carcinoma," *Journal of Clinical Oncology*, vol. 36, no. 36, Article ID Jco2018792549, 2018.

[4] J. Liu, P. D. Hanavan, K. Kras et al., "Loss of SETD2 induces a metabolic switch in renal cell carcinoma cell lines toward enhanced oxidative phosphorylation," *Journal of Proteome Research*, vol. 18, no. 1, pp. 331–340, 2019.

[5] P. Makhov, S. Joshi, P. Ghatalia, A. Kutikov, R. G. Uzzo, and V. M. Kolenko, "Resistance to systemic therapies in clear cell renal cell carcinoma: mechanisms and management strategies," *Molecular Cancer Therapeutics*, vol. 17, no. 7, pp. 1355–1364, 2018.

[6] J. Yu, W. Mao, B. Xu, and M. Chen, "Construction and validation of an autophagy-related long noncoding RNA signature for prognosis prediction in kidney renal clear cell carcinoma patients," *Cancer Medicine*, vol. 10, no. 7, pp. 2359–2369, 2021.

[7] H. Li, J. Hu, A. Yu et al., "RNA modification of N6-methyladenosine predicts immune phenotypes and therapeutic opportunities in kidney renal clear cell carcinoma," *Frontiers in Oncology*, vol. 11, Article ID 642159, 2021.

[8] Q. Luo and T. A. Vögeli, "Reclassification of kidney clear cell carcinoma based on immune cell gene-related DNA cpg Pairs," *Biomedicines*, vol. 9, no. 2, 2021.

[9] Y. Xiong, Z. Wang, Q. Zhou et al., "Identification and validation of dichotomous immune subtypes based on intratumoral immune cells infiltration in clear cell renal cell carcinoma patients," *Journal for Immunotherapy of Cancer*, vol. 8, no. 1, 2020.

[10] V. Pietrobon, "Cancer metabolism," *Journal of Translational Medicine*, vol. 19, no. 1, p. 87, 2021.

[11] R. M. Pascale, D. F. Calvisi, M. M. Simile, C. F. Feo, and F. Feo, "The warburg effect 97 years after its discovery," *Cancers*, vol. 12, no. 10, 2020.

[12] W. Sukjoi, J. Ngamkham, P. V. Attwood, and S. Jitrapakdee, "Targeting cancer metabolism and current anti-cancer drugs," *Advances in Experimental Medicine and Biology*, vol. 1286, pp. 15–48, 2021.

[13] D. J. Sanchez and M. C. Simon, "Genetic and metabolic hallmarks of clear cell renal cell carcinoma," *Biochimica Biophysica Acta Reviews on Cancer*, vol. 1870, no. 1, pp. 23–31, 2018.

[14] D. R. Crooks and W. M. Linehan, "The warburg effect in hominis: isotope-resolved metabolism in ccRCC," *Nature Reviews Urology*, vol. 15, no. 12, pp. 731-732, 2018.

[15] Y. Yang, C. Wang, N. Wei et al., "Identification of prognostic chromatin-remodeling genes in clear cell renal cell carcinoma," *Aging*, vol. 12, no. 24, pp. 25614–25642, 2020.

[16] P. Liu and W. Tian, "Identification of DNA methylation patterns and biomarkers for clear-cell renal cell carcinoma by multi-omics data analysis," *PeerJ*, vol. 8, Article ID e9654, 2020.

[17] Y. Wu, W. Han, D. Xu et al., "Identification of subtype specific biomarkers of clear cell renal cell carcinoma using random forest and greedy algorithm," *Biosystems*, vol. 204, Article ID 104372, 2021.

[18] X. Guo, Z. Sun, S. Jiang, X. Jin, and H. Wang, "Identification and validation of a two-gene metabolic signature for survival prediction in patients with kidney renal clear cell carcinoma," *Aging*, vol. 13, no. 6, pp. 8276–8289, 2021.

[19] G. Sokratous, S. Polyzoidis, and K. Ashkan, "Immune infiltration of tumor microenvironment following immunotherapy for glioblastoma multiforme," *Human Vaccines & Immunotherapeutics*, vol. 13, no. 11, pp. 2575–2582, 2017.

[20] G. Del Zotto, E. Marcenaro, P. Vacca et al., "Markers and function of human NK cells in normal and pathological conditions," *Cytometry Part B: Clinical Cytometry*, vol. 92, no. 2, pp. 100–114, 2017.

[21] I. Terrén, A. Orrantia, J. Vitallé, O. Zenarruzabeitia, and F. Borrego, "NK cell metabolism and tumor microenvironment," *Frontiers in Immunology*, vol. 10, p. 2278, 2019.

[22] C. M. Rice, L. C. Davies, J. J. Subleski et al., "Tumour-elicited neutrophils engage mitochondrial metabolism to circumvent nutrient limitations and maintain immune suppression," *Nature Communications*, vol. 9, no. 1, p. 5099, 2018.

[23] B. E. Hsu, Y. Shen, and P. M. Siegel, "Neutrophils: orchestrators of the malignant phenotype," *Frontiers in Immunology*, vol. 11, p. 1778, 2020.

[24] B. Chen, M. S. Khodadoust, C. L. Liu, A. M. Newman, and A. A. Alizadeh, "Profiling tumor infiltrating immune cells with CIBERSORT," *Methods in Molecular Biology*, vol. 1711, pp. 243–259, 2018.

[25] M. C. A. Wouters and B. H. Nelson, "Prognostic significance of tumor-infiltrating B cells and plasma cells in human cancer," *Clinical Cancer Research*, vol. 24, no. 24, pp. 6125–6135, 2018.

[26] G. Abril-Rodriguez and A. Ribas, "SnapShot: immune checkpoint inhibitors," *Cancer Cell*, vol. 31, no. 6, p. 848, 2017.

[27] Q. Wang, J. Zhang, H. Tu et al., "Soluble immune checkpoint-related proteins as predictors of tumor recurrence, survival, and T cell phenotypes in clear cell renal cell carcinoma patients," *Journal for ImmunoTherapy of Cancer*, vol. 7, no. 1, p. 334, 2019.

[28] R. Possemato, K. M. Marks, Y. D. Shaul et al., "Functional genomics reveal that the serine synthesis pathway is essential in breast cancer," *Nature*, vol. 476, no. 7360, pp. 346–350, 2011.

[29] S. R. Rosario, M. D. Long, H. C. Affronti, A. M. Rowsam, K. H. Eng, and D. J. Smiraglia, "Pan-cancer analysis of transcriptional metabolic dysregulation using the cancer genome atlas," *Nature Communications*, vol. 9, no. 1, p. 5330, 2018.

[30] Y. Yuan, J. Chen, J. Wang et al., "Development and clinical validation of a novel 4-gene prognostic signature predicting survival in colorectal cancer," *Frontiers in Oncology*, vol. 10, p. 595, 2020.

[31] G. Lucarelli, D. Loizzo, R. Franzin et al., "Metabolomic insights into pathophysiological mechanisms and biomarker discovery in clear cell renal cell carcinoma," *Expert Review of Molecular Diagnostics*, vol. 19, no. 5, pp. 397–407, 2019.

[32] R. H. Weiss, "Metabolomics and metabolic reprogramming in kidney cancer," *Seminars in Nephrology*, vol. 38, no. 2, pp. 175–182, 2018.

[33] M. Xiang, F. Du, J. Dai et al., "Exploring serum metabolic markers for the discrimination of ccRCC from renal angiomyolipoma by metabolomics," *Biomarkers in Medicine*, vol. 14, no. 8, pp. 675–682, 2020.

[34] R. Teng, Z. Liu, H. Tang et al., "HSP60 silencing promotes warburg-like phenotypes and switches the mitochondrial function from ATP production to biosynthesis in ccRCC cells," *Redox Biology*, vol. 24, Article ID 101218, 2019.

[35] S. Ergün, S. Güneş, R. Büyükalpelli, and O. Aydın, "Glutamate transporter SLC1A1 is associated with clear cell renal cell carcinoma," *Turkish Journal of Medical Sciences*, vol. 49, no. 2, pp. 531–537, 2019.

[36] Q. Peng, L. Wang, D. Zhao et al., "Overexpression of FZD1 is associated with a good prognosis and resistance of sunitinib in clear cell renal cell carcinoma," *Journal of Cancer*, vol. 10, no. 5, pp. 1237–1251, 2019.

[37] Y. Chen, J. He, C. Su et al., "LINC00461 affects the survival of patients with renal cell carcinoma by acting as a competing endogenous RNA for microRNA-942," *Oncology Reports*, vol. 42, no. 5, pp. 1924–1934, 2019.

[38] P. Kulkarni, P. Dasgupta, N. S. Bhat et al., "Elevated miR-182-5p associates with renal cancer cell mitotic arrest through diminished MALAT-1 expression," *Molecular Cancer Research*, vol. 16, no. 11, pp. 1750–1760, 2018.

[39] Z. X. Li, Q. N. Zhu, H. B. Zhang, Y. Hu, G. Wang, and Y. S. Zhu, "MALAT1: a potential biomarker in cancer," *Cancer Management and Research*, vol. 10, pp. 6757–6768, 2018.

[40] S. Qian, S. Sun, L. Zhang et al., "Integrative analysis of DNA methylation identified 12 signature genes specific to metastatic ccRCC," *Frontiers in Oncology*, vol. 10, Article ID 556018, 2020.

[41] Y. Wang, Y. Chen, B. Zhu, L. Ma, and Q. Xing, "A novel nine apoptosis-related genes signature predicting overall survival for kidney renal clear cell carcinoma and its associations with

immune infiltration," *Frontiers in Molecular Biosciences*, vol. 8, Article ID 567730, 2021.

[42] M. G. Vander Heiden and R. J. DeBerardinis, "Understanding the intersections between metabolism and cancer biology," *Cell*, vol. 168, no. 4, pp. 657–669, 2017.

[43] K. D. Courtney, D. Bezwada, T. Mashimo et al., "Isotope tracing of human clear cell renal cell carcinomas demonstrates suppressed glucose oxidation in vivo," *Cell Metabolism*, vol. 28, no. 5, pp. 793–800, 2018.

[44] L. Shi, S. An, Y. Liu, J. Liu, and F. Wang, "PCK1 regulates glycolysis and tumor progression in clear cell renal cell carcinoma through LDHA," *OncoTargets and Therapy*, vol. 13, pp. 2613–2627, 2020.

[45] Y. Xiao and D. Meierhofer, "Glutathione metabolism in renal cell carcinoma progression and implications for therapies," *International Journal of Molecular Sciences*, vol. 20, no. 15, 2019.

[46] O. D. K. Maddocks, D. Athineos, E. C. Cheung et al., "Modulating the therapeutic response of tumours to dietary serine and glycine starvation," *Nature*, vol. 544, no. 7650, pp. 372–376, 2017.

[47] Y. Liu, X. Liang, W. Dong et al., "Tumor-repopulating cells induce PD-1 expression in CD8(+) T cells by transferring kynurenine and AhR activation," *Cancer Cell*, vol. 33, no. 3, pp. 480–494, 2018.

[48] H. Miess, B. Dankworth, A. M. Gouw et al., "The glutathione redox system is essential to prevent ferroptosis caused by impaired lipid metabolism in clear cell renal cell carcinoma," *Oncogene*, vol. 37, no. 40, pp. 5435–5450, 2018.

[49] B. Allard, D. Allard, L. Buisseret, and J. Stagg, "The adenosine pathway in immuno-oncology," *Nature Reviews Clinical Oncology*, vol. 17, no. 10, pp. 611–629, 2020.

[50] S. Chevrier, J. H. Levine, V. R. T. Zanotelli et al., "An immune atlas of clear cell renal cell carcinoma," *Cell*, vol. 169, no. 4, pp. 736–749, 2017.

[51] L. T. Roumenina, M. V. Daugan, R. Noé et al., "Tumor cells hijack macrophage-produced complement C1q to promote tumor growth," *Cancer Immunology Research*, vol. 7, no. 7, pp. 1091–1105, 2019.

[52] X. Hua, J. Chen, Y. Su, and C. Liang, "Identification of an immune-related risk signature for predicting prognosis in clear cell renal cell carcinoma," *Aging*, vol. 12, no. 3, pp. 2302–2332, 2020.

[53] A. Sarvaria, J. A. Madrigal, and A. Saudemont, "B cell regulation in cancer and anti-tumor immunity," *Cellular & Molecular Immunology*, vol. 14, no. 8, pp. 662–674, 2017.

[54] L. Meng, Z. Tian, X. Long et al., "Caspase 4 overexpression as a prognostic marker in clear cell renal cell carcinoma: a study based on the cancer genome atlas data mining," *Frontiers in Genetics*, vol. 11, Article ID 600248, 2020.

[55] W. H. Fridman, L. Zitvogel, C. Sautès–Fridman, and G. Kroemer, "The immune contexture in cancer prognosis and treatment," *Nature Reviews Clinical Oncology*, vol. 14, no. 12, pp. 717–734, 2017.

[56] P. Darvin, S. M. Toor, V. Sasidharan Nair, and E. Elkord, "Immune checkpoint inhibitors: recent progress and potential biomarkers," *Experimental & Molecular Medicine*, vol. 50, no. 12, pp. 1–11, 2018.

[57] J. Luo, Y. Xie, Y. Zheng et al., "Comprehensive insights on pivotal prognostic signature involved in clear cell renal cell carcinoma microenvironment using the ESTIMATE algorithm," *Cancer Medicine*, vol. 9, no. 12, pp. 4310–4323, 2020.

[58] C. M. Robinson, B. P. K. Poon, Y. Kano, F. G. Pluthero, W. H. A. Kahr, and M. Ohh, "A hypoxia-inducible HIF1-GAL3ST1-sulfatide axis enhances ccRCC immune evasion via increased tumor cell-platelet binding," *Molecular Cancer Research*, vol. 17, no. 11, pp. 2306–2314, 2019.

[59] P. J. Siska, K. E. Beckermann, F. M. Mason et al., "Mitochondrial dysregulation and glycolytic insufficiency functionally impair CD8 T cells infiltrating human renal cell carcinoma," *JCI Insight*, vol. 2, p. 12, 2017.

[60] Q. Fu, L. Xu, Y. Wang et al., "Tumor-associated macrophage-derived interleukin-23 interlinks kidney cancer glutamine addiction with immune evasion," *European Urology*, vol. 75, no. 5, pp. 752–763, 2019.

[61] H. Nilsson, D. Lindgren, H. Axelson et al., "Features of increased malignancy in eosinophilic clear cell renal cell carcinoma," *The Journal of Pathology*, vol. 252, no. 4, pp. 384–397, 2020.